Fuel 406 (2026) 137033

Contents lists available at ScienceDirect

Fuel

journal homepage: www.elsevier.com/locate/fuel

Review article

Geochemical signatures, hydrocarbon generation kinetics, and oil-source correlation of the Es4 member source rocks in the Liaohe Western depression: implications for tight oil exploration in continental rift basins

Zhushi Ge [a,b], Xiaoping Liu [a,b,*], Xiaoguang Li [c], Yongcheng Chen [c], Chang Chen [c], Zilong Zhang [a,b], Biao Sun [a,b], Yi Zhong [a,b], Xueyou Tan [d], Gaohang Jia [a,b], Yu Xia [a,b], Zuowei Li [a,b], Wenhui Xie [a,b], Yu Yuan [a,b], Na Gao [a,b]

[a] College of Geosciences, China University of Petroleum (Beijing), Beijing 102249, China
[b] State Key Laboratory of Petroleum Resources and Engineering, Beijing 102249, China
[c] Liaohe Oilfield Exploration and Development Research Institute, Panjin 124010, China
[d] Geophysical Exploration Academy of China Metallurgical Geology Bureau, Baoding 071051, China

ARTICLE INFO

Keywords:
Liaohe Western Depression
Hydrocarbon generation kinetics
Geochemical characterization
Oil-source correlation
Tight oil

ABSTRACT

This study investigates the hydrocarbon generation potential and oil-source relationships of the Paleogene Shahejie Formation (Es4 Member) source rocks in the Leijia area, Liaohe Western Depression, through an integrated organic geochemical and hydrocarbon generation kinetic approach. Rock-Eval pyrolysis, biomarker analysis, stable carbon isotope analysis, and activation energy measurements were employed to characterize the geochemical signatures of the Es4d3 and Es4g submembers. The Es4d3 submember exhibits high organic matter richness, Type I–II_1 kerogen, low activation energy and early oil-generation capability under immature to low-maturity conditions, indicative of deposition in a highly reducing, deep lacustrine environment. In contrast, the Es4g submember shows higher organic matter abundance, Type II_1 kerogen, elevated activation energy, and predominant low-maturity stage, suggesting a weakly reducing, brackish lacustrine setting. A hierarchical cluster analysis confirms a strong genetic linkage between the crude oils and the Es4d3 source rocks, attributed to its low activation energy promoting early hydrocarbon expulsion. Comparative analysis with global analogs (e.g., Bakken, Vaca Muerta) highlights that lacustrine source rocks with low activation energy can efficiently generate hydrocarbons at low maturity, providing a novel indicator for tight oil exploration in continental basins. This work expands the effective source rock distribution of the Es4 Member, defines "sweet spot" targeting criteria, and offers insights for low-maturity oil exploration in analogous basins worldwide.

1. Introduction

With the global strategic transition of hydrocarbon exploration toward unconventional resources, tight oil has emerged as a critical successor to conventional reservoirs [1]. North America leads this domain, where the commercial success of the Bakken Formation in the Williston Basin has established a benchmark for unconventional hydrocarbon development worldwide [2]. Driven by this paradigm, breakthroughs have been achieved in both lacustrine (e.g., the Duvernay Formation, Canada) and marine (e.g., the Vaca Muerta Formation, Argentina) tight oil systems [3,4]. Recent geological surveys in China have revealed considerable tight oil reserves within the Tarim and Sichuan Basins, with promising development potential. [5,6]. However, oil-source correlation remains a key technical bottleneck, as traditional geochemical proxies (e.g., Pr/Ph ratios, sterane parameters) exhibit significant ambiguities under multi-charging events, biodegradation, and reservoir alteration [7,8]. Recent advances propose multi-proxy approaches—integrating biomarkers, isotopic signatures, and thermal modeling—to mitigate correlation uncertainties Peters et al. [9,10,11]. Nevertheless, the application of such integrated methodologies in complex lacustrine petroleum systems, particularly those with heterogeneous source-reservoir configurations, remains underexplored and warrants systematic investigation.

The third and fourth members of the Shahejie Formation (Es3-Es4) in

* Corresponding author at: College of Geosciences, China University of Petroleum (Beijing), Beijing 102249, China.
E-mail address: liuxiaoping@cup.edu.cn (X. Liu).

https://doi.org/10.1016/j.fuel.2025.137033
Received 13 June 2025; Received in revised form 26 August 2025; Accepted 29 September 2025
Available online 14 October 2025

the Leijia area, Liaohe Western Depression, host multiple lacustrine source rock intervals, representing critical targets for tight oil exploration in eastern China. While previous studies have focused on reservoir diagenesis [12] and resource potential evaluation [13], three key challenges impede reliable oil-source correlation: (1) biodegradation-induced distortion of geochemical parameters, (2) limited systematic core data from source rock intervals, and (3) complex overprinting effects from multi-phase hydrocarbon charging ([14]). Compared to well-characterized global tight oil systems such as the Bakken Formation (USA) and Cooper Basin (Australia), the Leijia area lacks robust constraints from hydrocarbon generation kinetics (e.g., activation energy distributions and thermal maturation thresholds), significantly hindering the precise delineation of exploration sweet spots. To resolve these challenges, we integrate: (i) biodegradation-resistant proxies (aromatic steroids, $\delta^{13}C$) to minimize distortion; (ii) systematic coring from 4 wells with multi-parameter validation for data robustness; and (iii) kinetic modeling combined with hierarchical clustering to deconvolve multi-charging effects.

This study focuses on the Es4 Member source rocks and associated crude oils in the Leijia area of the Liaohe Depression, employing an innovative integration of organic geochemistry (biomarkers, carbon isotopes) and hydrocarbon generation kinetics (activation energy analysis). We systematically characterize the differences in organic matter abundance, type, maturity and generative potential between the Es4d3 and Es4g sub-members. By benchmarking against global hydrocarbon generation models from both lacustrine and marine systems—such as the Bakken Formation and Vaca Muerta Formation (Argentina)—this work elucidates the oil-source relationships within the Liaohe tight oil system. The objectives of this research are threefold: (1) To develop a multi-parameter oil-source correlation model, resolving ambiguities inherent to conventional geochemical proxies, (2) To clarify the activation energy characteristics of the Es4 Member source rocks and their mechanistic role in low-maturity oil accumulation, (3) To establish a geochemical-kinetic evaluation framework for tight oil exploration in continental lacustrine basins, providing a transferable methodology for analogous basins worldwide.

2. Regional geological setting

The Liaohe western Depression, the largest hydrocarbon-generating sag in the Bohai Bay Basin, covers an area of approximately 2530 km^2 and exhibits a NE-trending structural framework characterized by "eastern faulting and western overlapping, steep eastern flank and gentle western slope", typical of a Meso-Cenozoic rift basin. It is subdivided into nine secondary structural units [15] (Fig. 1). The study area, located in the central-northern part of the depression (Leijia area), encompasses the northern Chenjia Sag, southern flank of the Gaosheng nose-shaped uplift, and northern segment of the Lengdong faulted anticline belt. The region is dominated by two fault systems: nearly E–W-trending and NE-trending. Early NE-trending faults were later cross-cut by E–W-trending faults, forming multi-level fault-block structures[16]. The Eocene Shahejie Formation Member 4 (Es4), overlying the Fangshenpao Formation, was deposited in a semi-closed lacustrine environment dominated by semi-deep to deep lacustrine fine-grained sediments. It is stratigraphically divided into the Dujiatai oil layer (upper) and Gaosheng oil layer (lower). The Dujiatai layer is further subdivided into three sub-members: Es4d1 (uppermost), Es4d2, and Es4d3 (lowermost). The Gaosheng sub-member (Es4g) represents deposition in a shallower lacustrine setting, with lithologies transitioning from mudstone interbedded with argillaceous dolomite (upper) to granular dolomite (base) (Fig. 2). During Dujiatai deposition, lake expansion culminated in the Es4d3 sub-member, characterized by thick analcime-bearing dolomite[17]. This study focuses on comparative geochemical characterization and hydrocarbon generation potential assessment of the Es4d3 and Es4g sub-members.

3. Samples and experimental

3.1. Samples

A total of 47 samples were collected from six wells in the Leijia area, Liaohe Basin (well locations shown in Fig. 1b), including: (1) 24 source rock samples from the Es4d3 sub-member: 17 samples from Well Le57; 7 samples from Well Le37. (2) 21 source rock samples from the Es4g sub-

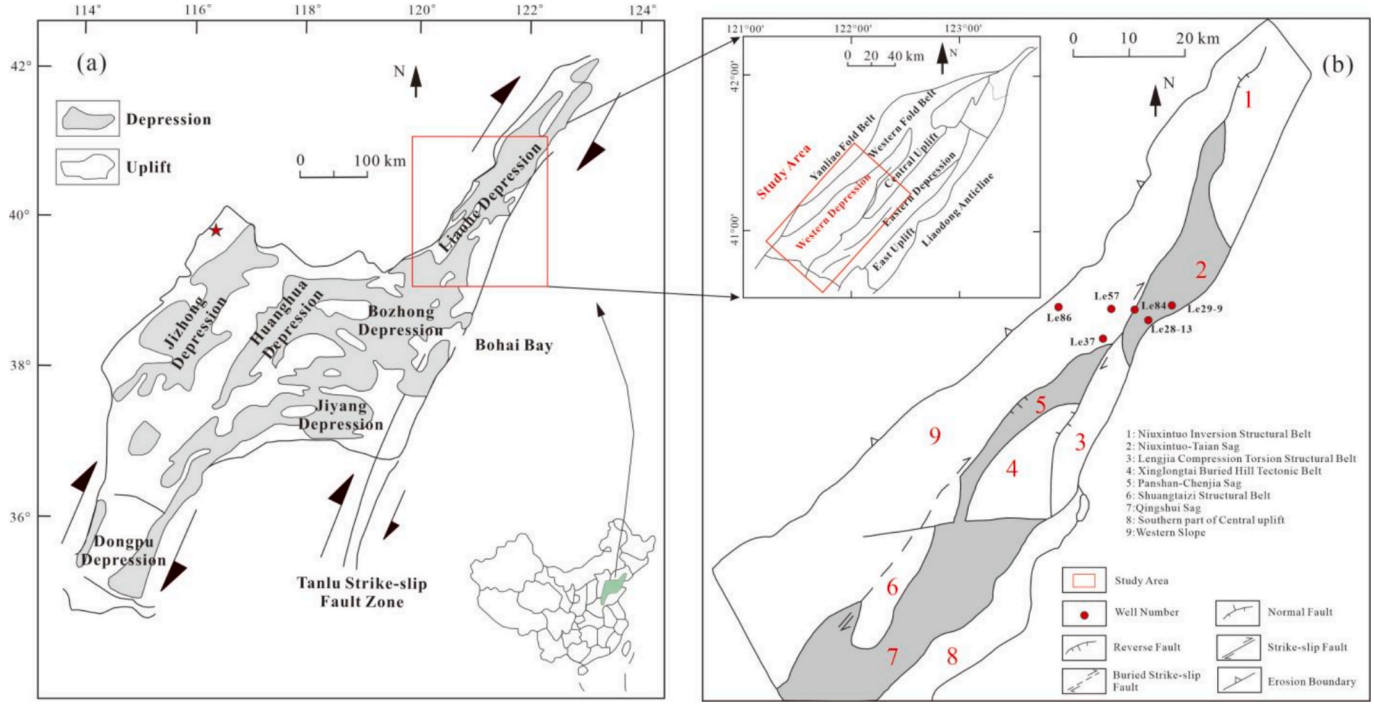

Fig. 1. Location map of the study area and sampling sites in the Liaohe Western Depression.(modified after [22]).

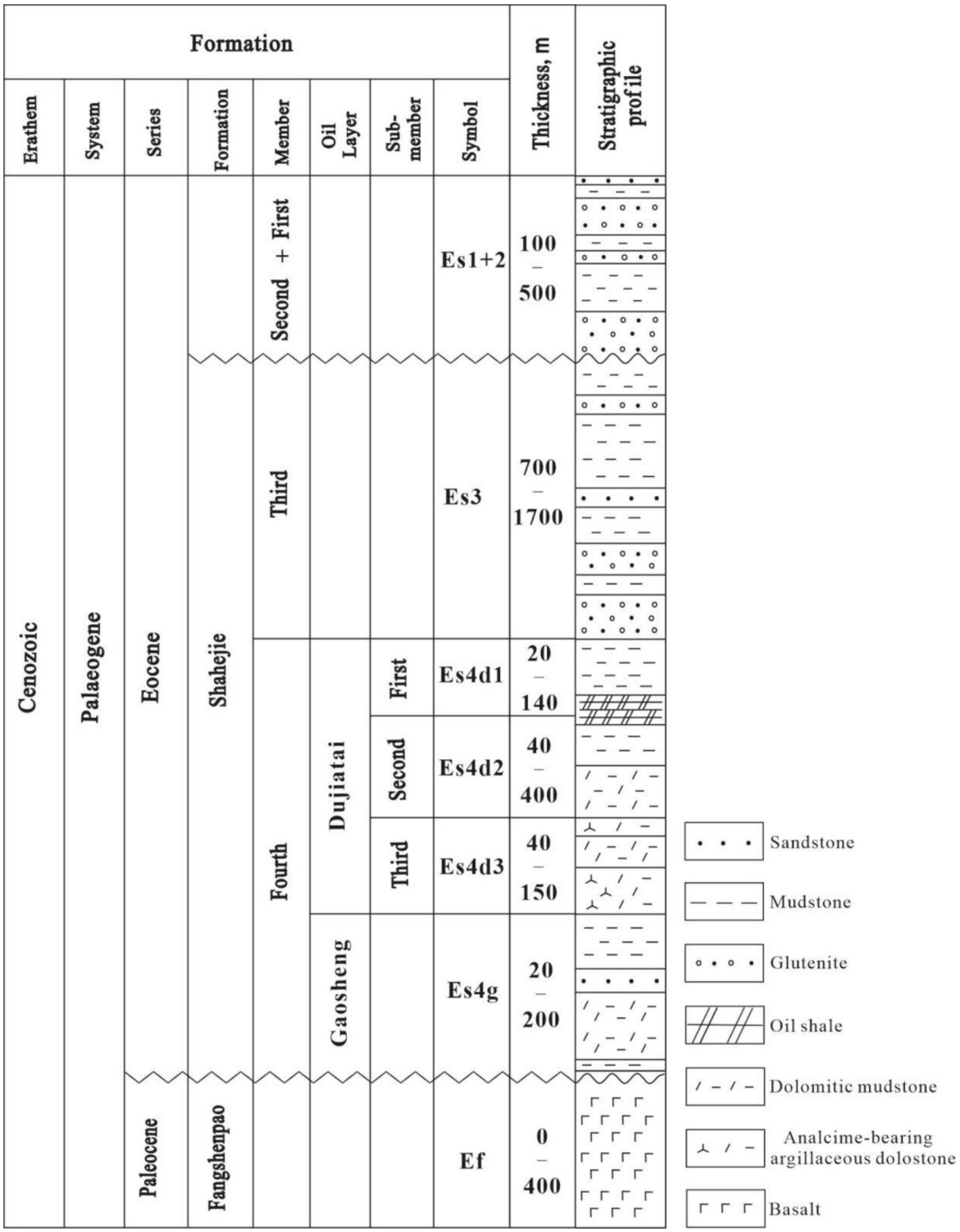

Fig. 2. Comprehensive stratigraphic column of the Liaohe Western Depression.

member: 19 samples from Well Le84; 2 samples from Well Le86. (3) 2 crude oil samples from the Es4 Member: 1 sample from Well Le29-9; 1 sample from Well Le28-13.

3.2. Total organic carbon (TOC)

Total organic carbon (TOC) analysis of shale samples followed a standardized protocol: crushed samples were sieved through a 200-mesh sieve and dried at 60°C under vacuum. A mass of 80 – 120 mg of powdered sample was weighed into a crucible and treated with 1:7 hydrochloric acid (prepared by mixing concentrated HCl with deionized water) to remove carbonate minerals. After HCl treatment, samples were repeatedly washed with deionized water until neutral pH, then oven-dried at 60 – 80 ℃. The decarbonated samples were subsequently combusted in a stream of high-purity oxygen at high temperature, converting total organic carbon to CO_2 gas which was quantified by infrared detection. Residual carbon was quantified using a LECO CS230 carbon–sulfur analyzer following GB/T 19145–2022 (*Determination of*

Organic Carbon in Sedimentary Rocks).

3.3. Rock pyrolysis analysis

Source rock samples were crushed to pass through a 200-mesh sieve and dried at 60 ℃ under reduced pressure. Approximately 100 mg of each sample was analyzed for pyrolytic properties using a Rock-Eval 6 pyrolyzer (France), following the protocol outlined in GB/T 18602–2012 (*Determination of Organic Matter in Sedimentary Rocks*). The analysis quantified three critical parameters: free hydrocarbons (S_1), pyrolyzed hydrocarbons (S_2), and maximum pyrolysis temperature (T_{max}).

3.4. Kerogen maceral identification

Kerogen maceral identification and quantitative analysis were conducted on a LEICA MPV-SP microphotometer following SY/T 6414–2014 (*Standard for Microscopic Component Identification and Quantification of Whole-Rock Slides*). Sample preparation included crushing rock fragments to 1.0 mm grain size, quartering to obtain representative subsamples, and impregnating with epoxy resin to form polished whole-rock slides. Quantitative maceral analysis employed a white-light and fluorescence combined point-counting method, with > 500 effective counting points per slide to determine the volumetric abundance of vitrinite, inertinite, and liptinite macerals.

3.5. Hydrocarbon generation kinetics experiment

To investigate the kinetic differences in hydrocarbon generation between the Es4g and Es4d3 sub-member, open-system pyrolysis experiments were conducted on one representative sample per subunit using a Rock-Eval 6 pyrolyzer. For Es4d3 (analcime-bearing dolomite), a sample from Well Le57 at 2363.8 m depth was selected; for Es4g (mudstone-dominated), a sample from Well Le84 at 2761.0 m depth was used. These samples were chosen based on their predominant lithology and representative geochemical characteristics (Table 1).

The tests employed three heating rates (5 ℃/min, 10 ℃/min, and 20 ℃/min), with an initial temperature of 200 ℃ and a final temperature of 700 ℃. Hydrocarbon generation parameters, including activation energy (E_a) and pre-exponential factor (A), were derived by applying a parallel first-order reaction model [18],Braun and Burnham [19] through Kinetic 2015 software. This model conceptualizes kerogen

Table 1
Organic geochemical characteristics of source rocks in the Es4 Member of the Liaohe Western Depression.

Well	Depth(m)	Formation	TOC (%)	S_1(mg/g)	S_2(mg/g)	$S_1 + S_2$ (mg/g)	HI (mg/g)	T_{max} (℃)	R_o (%)	$\delta^{13}C_{Kerogen}$ (‰)
Le57	2344.4	Es4d3	2.87	0.46	14.71	15.17	513	429	/	/
Le57	2346.3	Es4d3	3.33	0.80	17.41	18.21	523	435	/	/
Le57	2347.6	Es4d3	5.69	2.04	27.93	29.97	491	434	0.38	/
Le57	2348.4	Es4d3	5.05	1.09	26.14	27.23	518	434	/	/
Le57	2349.4	Es4d3	2.35	1.71	12.14	13.85	517	426	/	/
Le57	2350.1	Es4d3	2.52	0.73	12.27	13.00	487	434	0.41	−27.11
Le57	2352.6	Es4d3	1.82	1.94	10.41	12.35	572	429	/	/
Le57	2354.6	Es4d3	6.49	1.77	34.35	36.12	529	437	/	/
Le57	2355.5	Es4d3	0.60	0.32	1.59	1.91	265	427	/	/
Le57	2358.4	Es4d3	2.73	2.27	15.17	17.44	556	431	/	/
Le57	2363.8	Es4d3	2.44	5.55	13.71	19.26	563	424	0.38	/
Le57	2365.9	Es4d3	4.18	2.70	24.76	27.46	592	437	0.39	−26.36
Le57	2371.6	Es4d3	4.71	0.87	22.37	23.24	475	432	/	/
Le57	2380.0	Es4d3	2.98	0.77	15.44	16.21	518	436	0.43	−27.69
Le57	2384.1	Es4d3	2.67	0.60	15.87	16.47	594	437	/	/
Le57	2397.8	Es4d3	3.14	0.36	16.73	17.09	533	432	0.54	−28.93
Le57	2447.7	Es4d3	3.16	0.33	18.26	18.59	578	435	/	−29.05
Le37	2605.3	Es4d3	3.06	0.10	12.39	12.49	405	438	/	/
Le37	2614.5	Es4d3	3.23	0.15	12.06	12.21	373	439	/	/
Le37	2700.5	Es4d3	4.72	0.99	29.20	30.19	619	438	0.51	−28.76
Le37	2710.8	Es4d3	4.99	0.25	29.58	29.83	593	435	/	/
Le37	2721.5	Es4d3	5.54	0.23	24.82	25.05	448	440	/	/
Le37	2810.0	Es4d3	3.62	0.15	20.64	20.79	570	438	/	/
Le37	2815.7	Es4d3	3.55	0.19	18.60	18.81	524	441	/	/
Le84	2761.0	Es4g	5.99	1.09	33.93	35.02	566	431	0.48	−24.86
Le84	2763.0	Es4g	4.10	0.30	18.91	19.21	461	429	/	/
Le84	2763.4	Es4g	4.16	0.32	19.18	19.50	461	433	/	/
Le84	2766.7	Es4g	5.35	0.61	27.36	27.97	511	432	/	/
Le84	2768.2	Es4g	6.16	1.05	32.77	33.82	532	438	0.55	/
Le84	2770.2	Es4g	6.88	1.14	37.22	38.36	541	442	/	/
Le84	2770.4	Es4g	7.54	1.56	40.79	42.35	541	441	/	/
Le84	2772.1	Es4g	7.77	1.45	40.20	41.65	517	434	/	/
Le84	2773.2	Es4g	3.78	0.20	15.13	15.33	400	432	/	/
Le84	2773.9	Es4g	6.85	1.57	33.42	34.99	488	437	0.49	/
Le84	2775.8	Es4g	4.86	2.33	26.45	28.78	544	439	/	/
Le84	2777.7	Es4g	6.87	1.76	34.92	36.68	508	435	/	/
Le84	2778.3	Es4g	5.89	1.32	30.47	31.79	517	443	/	/
Le84	2780.0	Es4g	4.78	0.84	25.20	26.04	527	438	0.58	−27.40
Le84	2781.0	Es4g	5.43	3.74	25.94	29.68	478	439	/	/
Le84	2782.4	Es4g	5.33	1.85	28.77	30.62	540	442	/	/
Le84	2782.8	Es4g	3.55	0.43	15.99	16.42	450	440	/	/
Le84	2783.8	Es4g	4.42	0.41	19.45	19.86	440	438	/	/
Le84	2785.6	Es4g	5.33	2.61	26.56	29.17	498	443	0.65	/
Le86	1656.8	Es4g	2.31	0.32	15.34	15.66	457	438	0.60	−27.30
Le86	1659.4	Es4g	2.42	0.36	16.85	17.21	486	440	/	/
SD		Es4d3 (n = 24)	1.34	–	–	7.54	78.05	4.43	–	–
		Es4g (n = 21)	1.49	–	–	8.50	41.13	4.05	–	–

Table footnote. SD: Standard deviation; n: sample size, "/" – Not detected, "–" – Not calculated.

cracking as multiple independent reactions occurring simultaneously, each characterized by distinct activation energies, which effectively resolves the heterogeneous chemical composition of Type-II kerogen dominant in our samples Schenk and Horsfield [20,21]. Moreover, this model has already been applied in the study area([15,22]).The primary uncertainty lies in the extrapolation from laboratory to geological time scales, which was mitigated by employing multiple heating rates.

3.6. Gas chromatography-mass spectrometry (GC–MS)

The molecular composition of saturated hydrocarbons and aromatics was analyzed using an Agilent 7890A-5975C GC–MS system, following GB/T 18606–2017 (Determination of Biomarkers in Sediments and Crude Oils by Gas Chromatography-Mass Spectrometry). Saturated hydrocarbons were separated on a HP-5MS column (30 m × 0.25 mm × 0.25 μm) under constant flow mode with helium carrier gas (1 mL/min). The temperature program initiated at 80 ℃ (held for 2 min), ramped to 180 ℃ at 8 ℃/min, and further increased to 290 ℃ at 2 ℃/min (held for 20 min). For aromatic hydrocarbons, a HP-5MS column (60 m × 0.25 mm × 0.25 μm) was used with splitless injection. The oven program started at 50 ℃ (1 min hold), increased to 120 ℃ at 20 ℃/min, and finally reached 310 ℃ at 3 ℃/min (25 min hold). Data acquisition was performed in full-scan mode with an electron ionization (EI) source (70 eV, 100 mA filament current) (Xiao et al., 2024).

3.7. Carbon isotope analysis

Carbon isotope ratios ($\delta^{13}C$) were measured using a DELTA Plus XL isotope ratio mass spectrometer. Sample preparation involved combusting aliphatic fractions in an elemental analyzer (EA) combustion furnace at ~ 980°C to produce CO_2, which was split-injected into the mass spectrometer. Helium carrier gas (He) was used for transport. Analytical conditions included an electron energy of 68 eV, emission current of 0.800 mA, mass resolution of 200, and a vacuum pressure $< 2 \times 10^{-6}$ Pa. Data were calibrated against the PDB standard, with $\delta^{13}C$ measurement uncertainties $\leq \pm 0.1$ ‰ [23].

4. Results

4.1. Rock-Eval pyrolysis characteristics

4.1.1. Organic matter abundance

Organic matter abundance, a critical parameter for evaluating generative potential, reflects the enrichment degree of organic material in source rocks. Key evaluation indices include Total Organic Carbon (TOC), pyrolytic hydrocarbon potential ($S_1 + S_2$), chloroform bitumen "A" and total hydrocarbon content (HC). This study prioritizes TOC and $S_1 + S_2$ for abundance assessment. The Es4d3 exhibits TOC values of 0.60 % – 6.49 % (average 3.56 %) and $S_1 + S_2$ values of 1.91 – 36.12 mg/g (average 19.70 mg/g), classifying it predominantly as excellent source rocks (Table 1 and Fig. 3a–b). The overlying Es4g demonstrates higher organic richness, with TOC ranging from 2.31 % to 7.77 % (average 5.23 %) and $S_1 + S_2$ from 15.33 to 42.35 mg/g (average 28.10 mg/g), also categorized as excellent source rocks (Table 1 and Fig. 3a).

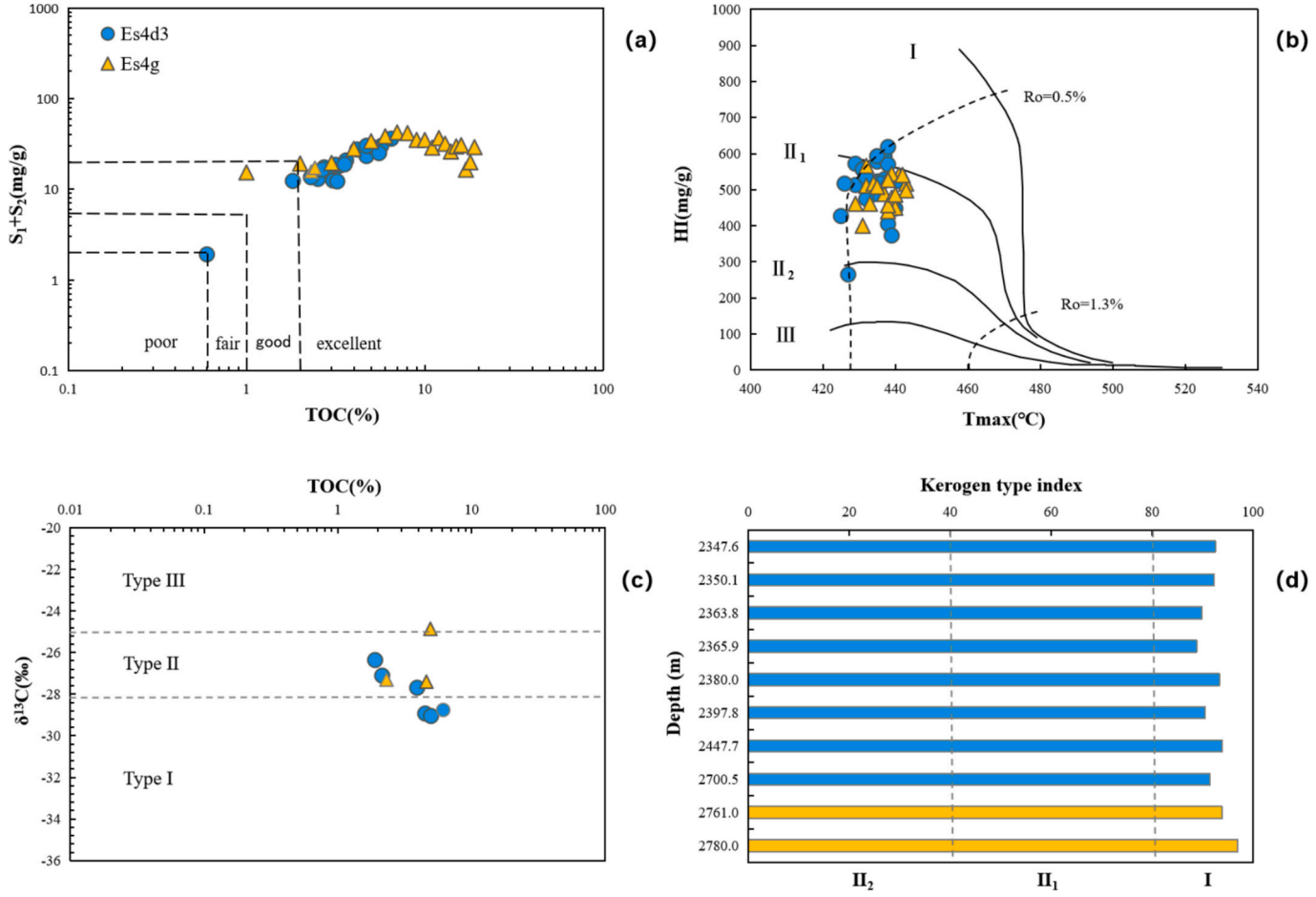

Fig. 3. Geochemical characteristics of the Es4 source rocks in the Liaohe Western Depression: (a) TOC vs. $S_1 + S_2$ cross-plot, (b) Tmax vs. HI cross-plot, (c) TOC vs. $\delta^{13}C$ cross-plot, and (d) kerogen typing diagram.

4.1.2. Organic matter type

The type of organic matter in source rocks is a critical factor controlling their oil-generation capability. Various classification schemes exist based on chemical composition and organic matter origin, such as the common tripartite scheme (Type I, II, III; Tissot and Welte [24,25], Panwar et al. [26], the three-category four-type scheme (Type I, II_1, II_2, III; Yang [27], and the quadripartite scheme (Type I, II, III, IV; [28,29], Nath et al. [30]. The three-category four-type scheme – Type I (Sapropelic), Type II_1 (Humic-Sapropelic), Type II_2 (Sapropelic-Humic), Type III (Humic) – is widely adopted in many Chinese oilfield studies and is applied herein.

Based on integrated analyses of pyrolysis hydrogen index (HI) and kerogen maceral composition, the two sets of source rocks in the Es4 Member exhibit distinct characteristics. For the Es4d3, the HI ranges from 265 to 619 mg HC/g TOC (average 515 mg HC/g TOC). Combined with kerogen maceral identification, these data indicate that the organic matter is predominantly Type II_1 with minor Type I contributions (Fig. 3b). The $\delta^{13}C$ values of kerogen range from −29.1 ‰ to −26.4 ‰ (average −28.0 ‰), further corroborating its sapropelic-humic mixed organic matter characteristics (Type I–II) (Fig. 3c). In contrast, the Es4g exhibits an HI range of 400 – 566 mg HC/g TOC (average 498 mg HC/g TOC) and maceral compositions consistent with Type II_1 organic matter (Fig. 3b). The relatively heavier $\delta^{13}C$ values (−27.4 ‰ to −24.9 ‰, average −26.1 ‰) suggest enhanced contributions from terrestrial higher plants. Cross-plots of T_{max} versus HI (Fig. 3c), combined with $\delta^{13}C$ and maceral composition analyses (Fig. 3d), reveal that the organic matter in the Es4d3 is classified as Type II_1 dominant with a minor contribution from Type I, whereas the Es4g is dominated by Type II_1 (Table 1). This discrepancy is closely linked to the evolution of sedimentary environments and variations in terrestrial organic input.

4.1.3. Organic matter maturity

Thermal maturity of the source rocks in the study area was evaluated using pyrolysis Tmax and vitrinite reflectance (R_o). For the Es4d3, T_{max} values range from 424 to 441 ℃ (average 434 ℃), and R_o values vary between 0.38 % and 0.54 % (average 0.44 %), indicating an immature to low-maturity stage. In contrast, the Es4g exhibits higher thermal maturity, with T_{max} values of 429 – 443 ℃ (average 437 ℃) and R_o values of 0.48 – 0.65 % (average 0.55 %), predominantly within the low-maturity stage (Table 1 and Fig. 3b). Overall, the Es4g demonstrates greater maturity than the Es4d3.

4.2. Compositional characteristics of biomarkers in source rocks and crude oils

4.2.1. N-alkanes and acyclic isoprenoids

The *n*-alkane distribution in the Es4d3 source rocks of the Liaohe Western Depression is predominantly unimodal with a rear-peak pattern (Fig. 4), where the main peak carbon is typically *n*-C_{23}. The Carbon Preference Index (CPI) ranges from 1.10 to 1.36 (average 1.20), and the Odd-Even Predominance (OEP) varies between 1.10 and 2.34 (average 1.42), indicating a pronounced odd-carbon predominance (Fig. 4 and Table 2). In contrast, the Es4g exhibits a bimodal *n*-alkane distribution, with main peaks spanning *n*-C_{17} to *n*-C_{27}. The average CPI and OEP values for this sub-member are both 1.23, also reflecting significant odd-carbon preference (Fig. 4 and Table 2).

Significant differences in Pr/Ph (pristane/phytane) ratios are observed between the two sub-members. For the Es4d3 (based on samples from Wells Le 57 and Le 37), phytane (Ph) predominates over adjacent *n*-alkanes (*n*-C_{18}), with Pr/Ph ratios consistently low (<0.40) (Table 2 and Fig. 4). This suggests deposition in a strongly reducing, saline environment. Conversely, the Es4g displays notably higher Pr/Ph ratios (up to 0.94), indicative of a less reducing depositional setting

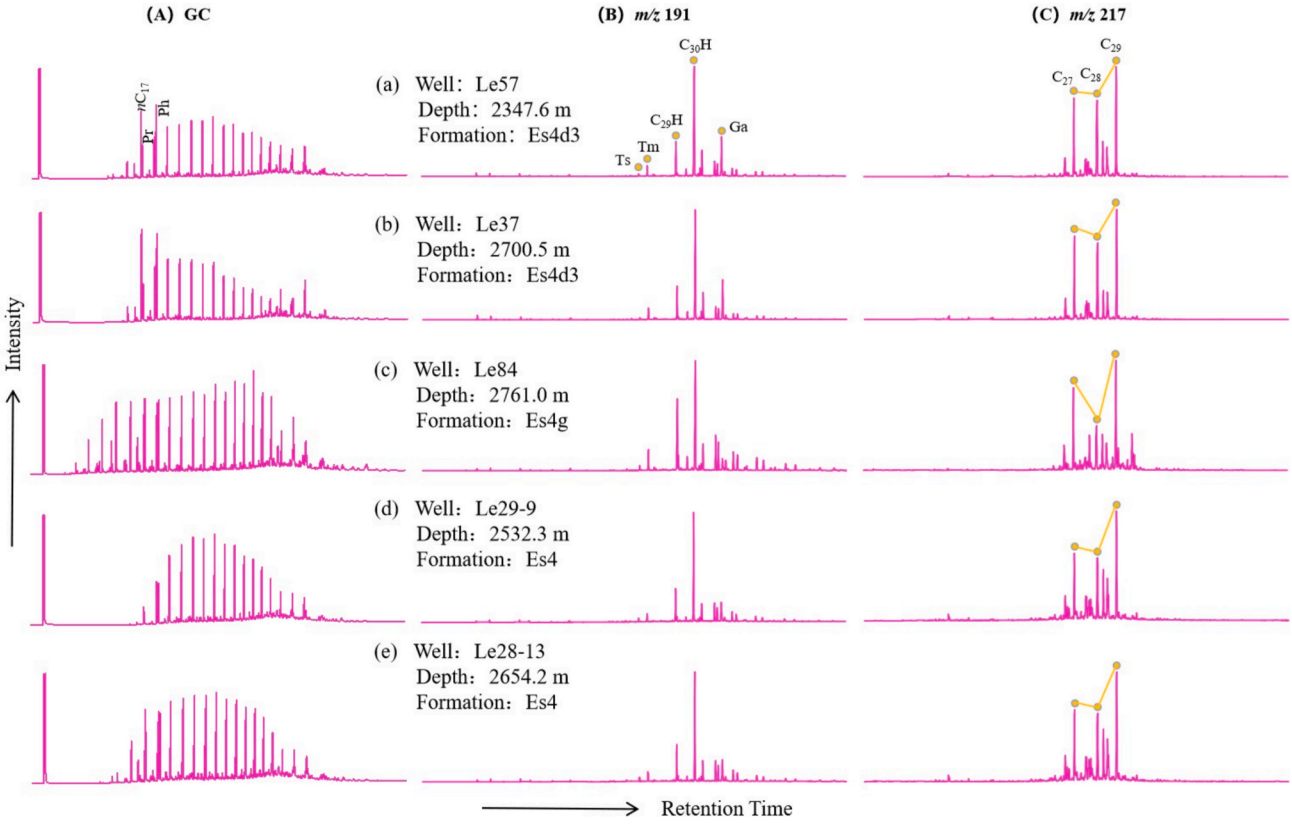

Fig. 4. Representative chromatograms of the Es4 source rocks (a–c) and crude oil sample (e) from the Liaohe Western Depression: (A) Whole-oil gas chromatography (GC) chromatogram, (B) *m/z* 191 terpenoids, and(C) *m/z* 217 steranes mass chromatograms.

Table 2
Composition of saturated hydrocarbon biomarkers in the Es4 source rocks and crude oils from the Liaohe Western Depression.

Well	Depth (m)	Formation	Main Peak	CPI	OEP	Pr/ *n*-C_{17}	Ph/ *n*-C_{18}	Pr/ Ph	C_{19-20}TT/ C_{21}TT	C_{19-23}TT /C_{30}H	Ts/ (Ts + Tm)	C_{30}RAH/ C_{29}Ts	Ga/ C_{31}H	C_{27} /C_{29} ααα	Sterane/ Hopane
Le57	2347.6	Es4d3	*n*-C_{23}	1.20	1.13	0.53	1.99	0.35	1.15	0.04	0.16	0.38	0.34	0.58	0.35
Le57	2350.1	Es4d3	*n*-C_{17}	1.20	2.22	0.64	1.97	0.44	1.06	0.05	0.16	0.36	0.35	0.60	0.34
Le57	2363.8	Es4d3	*n*-C_{23}	1.19	1.15	0.72	2.45	0.30	1.04	0.03	0.16	0.41	0.31	0.59	0.42
Le57	2365.9	Es4d3	*n*-C_{23}	1.19	1.14	0.68	2.28	0.37	1.11	0.04	0.15	0.37	0.33	0.60	0.38
Le57	2380.0	Es4d3	*n*-C_{23}	1.36	1.15	1.01	3.14	0.35	1.04	0.04	0.11	0.03	0.36	0.16	0.31
Le57	2397.8	Es4d3	*n*-C_{23}	1.13	1.16	1.15	3.33	0.18	1.23	0.06	0.10	0.35	0.56	0.58	1.20
Le57	2447.7	Es4d3	*n*-C_{27}	1.10	1.10	0.60	1.60	0.47	1.22	0.04	0.11	0.23	0.55	0.62	0.19
Le37	2700.5	Es4d3	*n*-C_{17}	1.21	2.34	0.57	1.70	0.35	1.19	0.05	0.15	0.29	0.39	0.63	0.39
Le84	2761.0	Es4g	*n*-C_{27}	1.24	1.29	0.93	1.08	0.94	0.99	0.04	0.17	0.25	0.12	0.63	0.22
Le84	2780.0	Es4g	*n*-C_{17}	1.21	1.16	0.59	0.95	0.77	0.93	0.07	0.16	0.42	0.68	0.59	0.17
Le86	1656.8	Es4g	/	/	/	/	/	/	0.81	0.03	0.21	0.57	0.45	0.50	0.27
Le29-9	2532.3	Es4	*n*-C_{23}	1.17	1.09	0.71	0.95	0.30	0.75	0.04	0.29	0.48	0.24	0.50	0.25
Le28-13	2654.2	Es4	*n*-C_{23}	1.18	1.08	0.72	0.94	0.29	0.83	0.05	0.28	0.50	0.24	0.52	0.26
SD		Es4d3 (n = 8)	–	–	–	–	–	0.08	0.07	–	–	–	0.09	0.15	0.29
		Es4g (n = 3)	–	–	–	–	–	0.09	0.07	–	–	–	0.23	0.05	0.04

Table footnote. CPI={(C_{25} + C_{27} + C_{29} + C_{31} + C_{33})[1/(C_{24} + C_{26} + C_{28} + C_{30} + C_{32})+1/(C_{26} + C_{28} + C_{30} + C_{32} + C_{34})]}/2; OEP = [(C_i + 6C_{i+2} + C_{i+4})/4(C_{i+1} + C_{i+3})]^m, i + 2: Main peak carbon, m: (−1) i + 1 ; Pr – Pristane; Ph – Phytane; TT – Tricyclic terpanes; H – Hopane; Ts – 18α(H)-C_{27} Trisnorneohopane; Tm – 18α(H)-C_{27} Trisnorhopane; RAH – Rearranged hopanes; Ga – Gammacerane; C_{27}/C_{29} ααα – C_{27} ααα-cholestane (20R)/C_{29} ααα-sterane (20R); SD: Standard deviation; n: sample size, "/" – Not detected, "–" – Not calculated.

(Fig. 4 and Table 2).

4.2.2. Terpanoids and steranes

Tricyclic terpanoids (TT), gammacerane (Ga), and hopanes (H) are detected in source rock samples from both sub-members of the Es4 Member in the Liaohe Western Depression (Fig. 4). Biomarker ratios are key indicators of organic matter source, depositional environment, and thermal maturity. To clarify the following discussion, key biomarker ratios are defined here at their first occurrence. For the Es4d3, the ratio of C_{19-20} tricyclic terpanes to C_{21} tricyclic terpane(C_{19-20}TT/C_{21}TT) commonly used to assess organic matter source, is notably high (1.04 – 1.23, average 1.13) (Fig. 4 and Table 2), while the atio of C_{19-23} tricyclic terpanes to C_{30} hopane (C_{19-23}TT/C_{30}H) another indicator of source input, is relatively low (0.03 – 0.06, average 0.04). The ratio of C_{30} rearranged hopane to C_{29} 18α(H)-30-Norneohopane (C_{30}RAH/C_{29}Ts) ranges from 0.03 to 0.41 (average 0.30), the ratio of gammacerane to C_{31} hopane (Ga/C_{31}H), a well-established indicator of depositional environment (specifically water column stratification and salinity), varies between 0.31 and 0.56 (average 0.40). In contrast, the Es4g exhibits a lower C_{19-20}TT/C_{21}TT ratio (0.81 – 0.99, average 0.96) but higher C_{19-23}TT/C_{30}H (0.03 – 0.07, average 0.05) and C_{30}RAH/C_{29}Ts ratios (0.25 – 0.57, average 0.30). The Ga/C_{31}H ratio in this sub-member spans 0.12 – 0.68 (average 0.40). Regular steranes (C_{27} – C_{29}) are widely identified in both sub-members, with C_{29} regular steranes dominating (Fig. 4). The atio of C_{27} to C_{29}ααα20R steranes (C_{27}/C_{29}ααα),used to evaluate organic matter source, shows a distribution pattern similar to the C_{30}RAH/C_{29}Ts ratio: lower in the Es4d3 and higher in the Es4g. Conversely, the sterane to hopane ratio (sterane/hopane),which can reflect source input and depositional conditions, displays an inverse trend (Fig. 4 and Table 2).

4.2.3. Aromatic compounds

GC–MS analysis of aromatic compounds in the Es4 source rocks from the Leijia area of the Liaohe Western Depression identified a variety of aromatic compounds, primarily including naphthalene (N), phenanthrene (P), dibenzothiophene (DBT), and triaromatic steroids (TAS), with phenanthrene and triaromatic steroid series dominating (Table 3 and Fig. 5). In the Es4d3, triaromatic steroid concentrations are relatively high, generally exceeding 60 %, whereas the Es4g exhibits lower TAS content. Phenanthrene concentrations follow a similar trend but remain comparatively low (typically < 25 %). Naphthalene distribution contrasts sharply between the sub-members: the Es4d3 shows lower naphthalene content, while the Es4g displays significantly higher values, often exceeding 50 % (Table 3 and Fig. 5).

4.2.4. Component-specific carbon isotopes

The stable carbon isotopic composition ($\delta^{13}C$) of the Es4 Member source rocks in the Liaohe Western Depression exhibits significant variability between sub-members (Fig. 6). For the Es4d3: Saturated hydrocarbons: $\delta^{13}C$ ranges from −34.7 ‰ to −30.8 ‰ (average –32.3 ‰). Aromatic hydrocarbons: $\delta^{13}C$ ranges from −30.0 ‰ to −28.8 ‰ (average −29.4 ‰). Non-hydrocarbons: $\delta^{13}C$ ranges from −30.0 ‰ to −28.0 ‰ (average −28.8 ‰). Asphaltenes: $\delta^{13}C$ ranges from −29.8 ‰ to −27.5 ‰ (average −28.4 ‰). The $\delta^{13}C$ values of soluble organic matter components in the Es4d3 follow the order: saturated hydrocarbons < aromatic hydrocarbons < non-hydrocarbons < asphaltenes, with an overall lighter isotopic composition (<-29 ‰).In contrast, the Es4g displays distinct isotopic trends: Saturated hydrocarbons: $\delta^{13}C$ ranges from –33.6 ‰ to −30.4 ‰ (average −31.0 ‰). Aromatic hydrocarbons: $\delta^{13}C$ ranges from −39.2 ‰ to −27.0 ‰ (average −28.2 ‰). Non-hydrocarbons: $\delta^{13}C$ ranges from −28.9 ‰ to −26.5 ‰ (average −27.7 ‰). Asphaltenes: $\delta^{13}C$ ranges from −28.3 ‰ to −27.6 ‰ (average −27.9 ‰). Here, the $\delta^{13}C$ sequence shifts to saturated hydrocarbons < asphaltenes < aromatic hydrocarbons < non-hydrocarbons, reflecting a heavier overall isotopic composition (>-29 ‰) (Fig. 6).

The marked isotopic differences between the sub-members likely

Table 3
Geochemical composition of aromatic hydrocarbons in the Es4 source rocks and crude oils from the Liaohe Western Depression.

Well	Depth (m)	Formation	9-MP/ 1-MP	F%	OF%	SF%	DBT/P	N%	P%	DBT%	TAS%
Le57	2347.6	Es4d3	1.42	13.91	5.62	80.47	0.04	3.14	36.51	0.12	60.24
Le57	2350.1	Es4d3	1.42	14.04	4.78	81.19	0.01	1.82	46.30	0.08	51.79
Le57	2363.8	Es4d3	1.42	53.16	14.20	32.65	0.05	0.59	8.29	0.21	90.91
Le57	2365.9	Es4d3	1.39	33.20	8.63	58.17	0.03	1.01	24.75	0.16	74.07
Le57	2380.0	Es4d3	1.41	31.09	8.93	59.98	0.05	2.23	11.34	0.20	86.23
Le57	2397.8	Es4d3	1.23	10.40	3.29	86.31	0.04	1.32	29.32	0.09	69.27
Le57	2447.7	Es4d3	1.09	43.56	12.18	44.27	0.03	0.52	25.86	0.17	73.45
Le37	2700.5	Es4d3	1.24	8.89	3.07	88.03	0.03	1.55	33.67	0.12	64.66
Le84	2761.0	Es4g	1.06	28.96	22.91	48.14	0.26	49.97	11.98	0.02	38.03
Le84	2780.0	Es4g	1.18	19.62	27.16	53.23	0.17	57.65	23.26	0.01	19.08
Le86	1656.8	Es4g	1.49	36.93	15.36	47.71	0.08	0.68	12.43	0.13	86.76
Le29-9	2532.3	Es4	1.30	63.74	14.97	21.29	0.05	1.29	30.64	0.14	67.93
Le28-13	2654.2	Es4	1.35	26.06	6.49	67.46	0.03	1.58	43.16	0.07	55.19

Table footnote. MP – Methylphenanthrene; F – Fluorene; OF – Oxyfluorene; SF – Thiofluorene; DBT – Dibenzothiophene; P – Phenanthrene; N – Naphthalene; TAS – Triaromatic steroids.

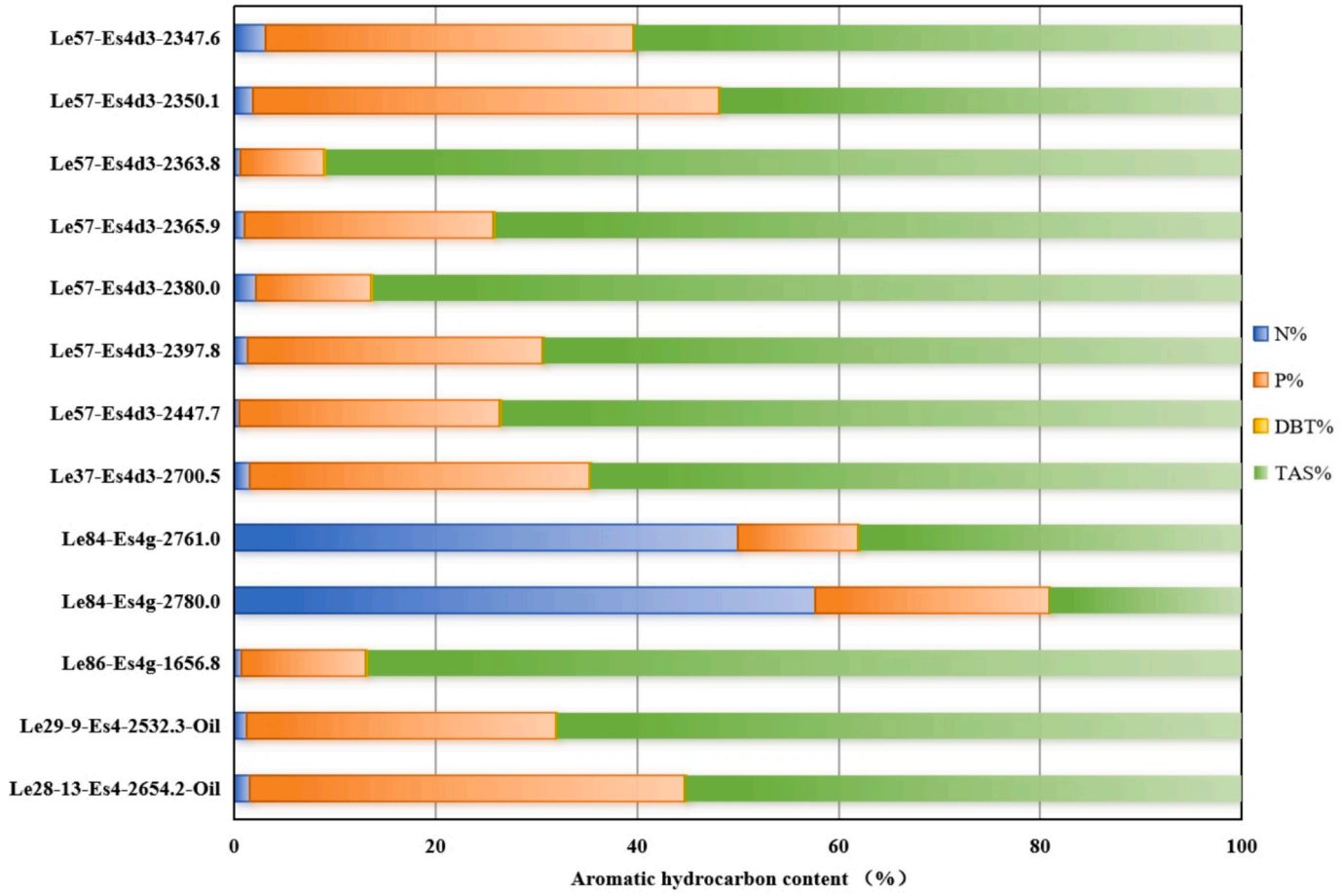

Fig. 5. Compositional characteristics of aromatic compounds in the Es4 source rocks and crude oils from the Liaohe Western Depression.

reflect variations in depositional environments and organic matter sources during the formation of the Es4 source rocks. Previous studies confirm that these rocks were deposited in semi-deep to deep lacustrine subfacies[31,32], where spatial heterogeneity in redox conditions, salinity, and terrestrial versus aquatic organic inputs may have driven the observed $\delta^{13}C$ variability.

4.3. Kinetic characteristics of hydrocarbon generation

Experimental results reveal distinct differences in the activation energy distributions of oil generation between the Es4d3 and Es4g, indicating divergent generation processes (Fig. 7). The Es4g exhibits later hydrocarbon generation onset and a shorter generation window, with a dominant activation energy peak at 56 kcal/mol (SD, 4.8 kcal/mol), reflecting a relatively concentrated generation phase (Fig. 7b and Fig. 7d). In contrast, the Es4d3 generates hydrocarbons earlier, with a prolonged generation period spanning the entire pyrolysis experiment. Its activation energy distribution displays a bimodal pattern (peaks at 48 kcal/mol and 58 kcal/mol) and a broader range (SD, 1.5 kcal/mol), suggesting the capacity to produce a proportion of low-maturity crude

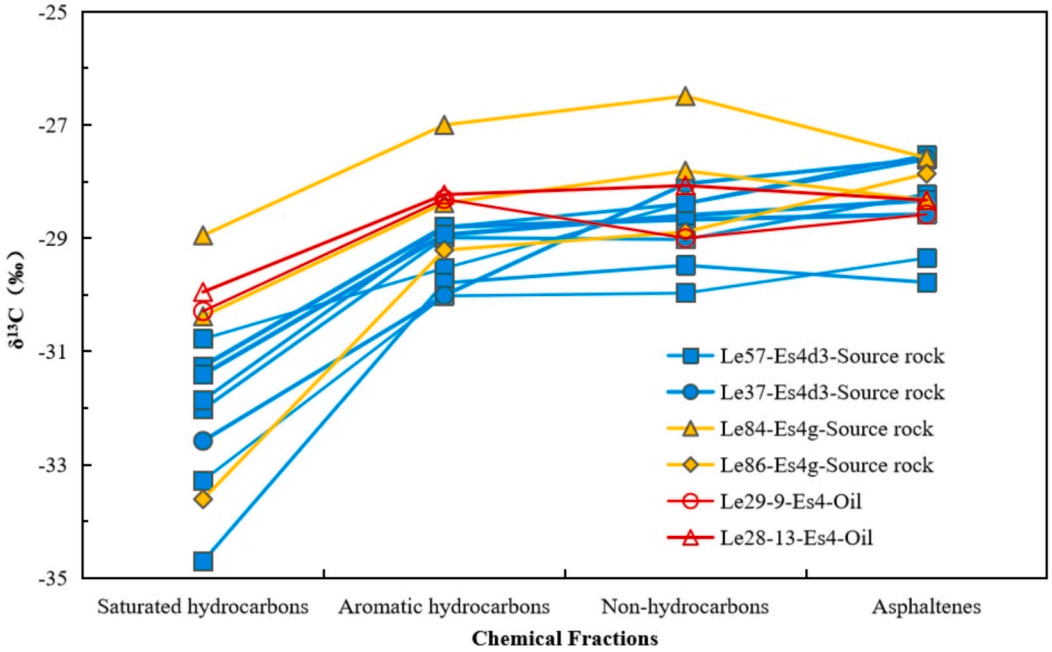

Fig. 6. Carbon isotopic composition ($\delta^{13}C$) of chemical fractions in the Es4 source rocks and crude oils from the Liaohe Western Depression.

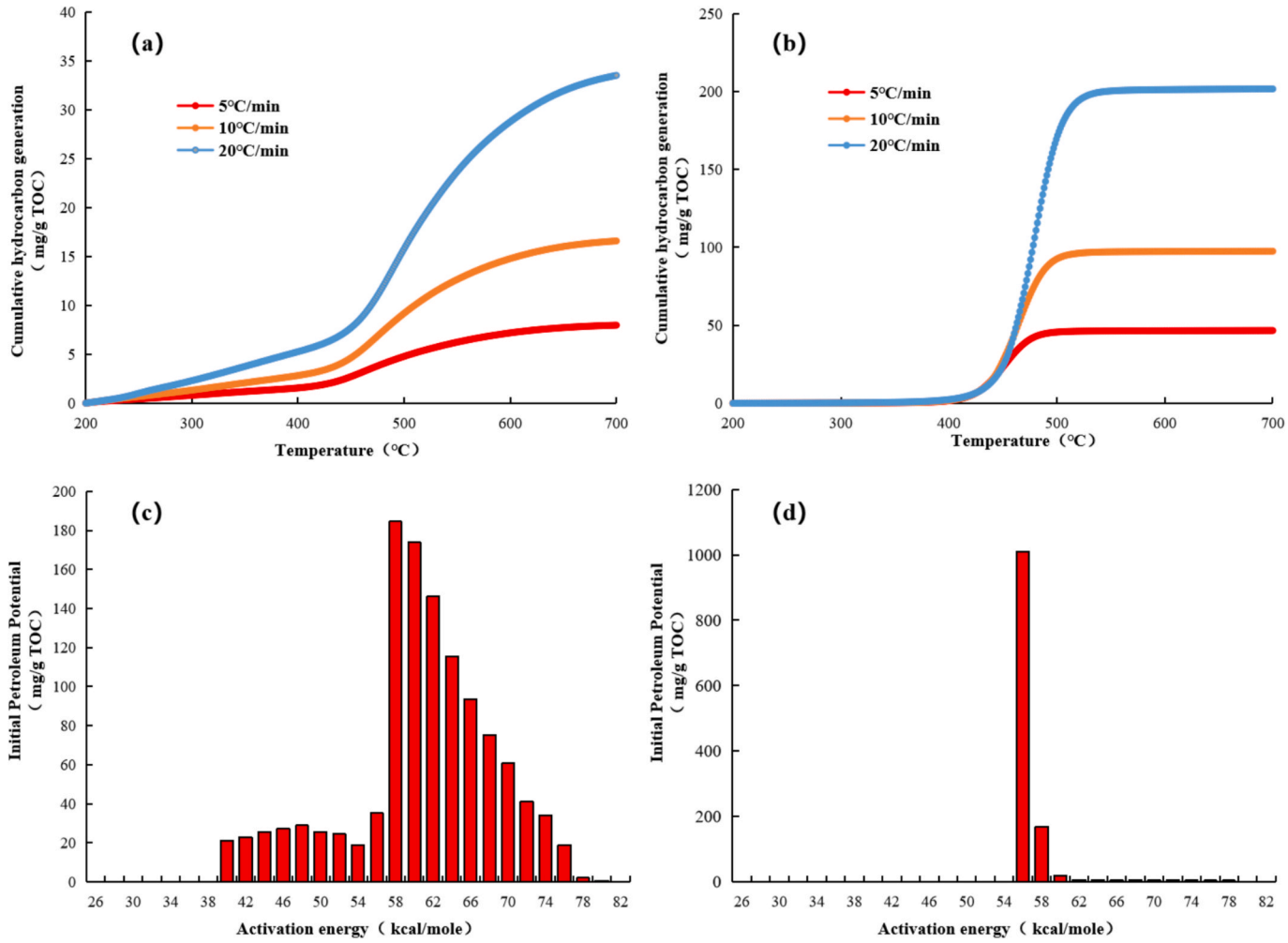

Fig. 7. Hydrocarbon generation kinetics experiments for the Es4 in the Liaohe Western Depression: (a) Cumulative hydrocarbon yield vs. temperature for the Es4d3; (b) Cumulative hydrocarbon yield vs. temperature for the Es4g; (c) Activation energy distribution of the Es4d3; (d) Activation energy distribution of the Es4g.

oil (Fig. 7a and Fig. 7c). This markedly different E_a distribution confirms that the analcime-bearing dolomite (Es4d3) and mudstone (Es4g), despite their spatial proximity, undergo fundamentally divergent oil generation processes. This phenomenon is a critical control on the relative timing of hydrocarbon generation and overpressure development in the study area and is increasingly recognized as a key feature of mixed lithology source rock systems [15]. The low-temperature hydrocarbon generation characteristics of the Es4d3 contrast sharply with those of the North American Bakken Shale (activation energy: 58–65 kcal/mol), highlighting the thermal instability advantage of lacustrine algal organic matter [33].

While the kinetic models provide a quantitative framework, direct extrapolation to geological time scales entails uncertainty. Multi-heating rate experiments reduce but do not eliminate the inherent limitations of open-system pyrolysis, particularly regarding confinement pressure. However, the strong consistency between kinetic results and biomarker evidence robustly supports the lithologically controlled charge model. Future integration with burial history modeling and pressure-correction methods will further refine predictive capability.

5. Discussion

5.1. Depositional environment

The Pr/Ph ratio is widely used to infer redox conditions during deposition: Pr/Ph < 0.8 indicates a strongly reducing environment, 0.8 – 3.0 reflects reducing conditions, and > 3.0 suggests oxidizing environments with enhanced terrestrial organic input Didyk et al. [34],Connan [35] ; [36]. In the Liaohe Western Depression, the Es4d3 source rocks exhibit low Pr/Ph ratios (0.18 – 0.47) (Table 2), indicating deposition in a strongly reducing environment. In contrast, the Es4g displays higher Pr/Ph ratios (0.77 – 0.94, average 0.86) (Table 2), consistent with deposition under reducing conditions.

Cross-plots of Pr/n-C_{17} versus Ph/n-C_{18} [37] further reveal environmental contrasts between the sub-members. The Es4g source rocks cluster in zones indicative of moderately reducing conditions with predominant aquatic organic matter inputs. In contrast, the Es4d3 plots within fields reflecting strongly reducing environments dominated by lacustrine algal organic matter (Fig. 8a). Elevated gammacerane indices ($Ga/C_{31}H$ = 0.31–0.56) confirm hypersaline water column conditions, consistent with interpretations from Pr/Ph and DBT/PHEN ratios [38,39]. Integration of multiple biomarker proxies demonstrates that both sub-members were deposited in saline deep to semi-deep lacustrine facies (Fig. 8b).

The depositional environmental differences between the Es4 sub-members are further reflected in aromatic hydrocarbon compositions. Thiofluorene (SF) typically forms under reducing to strongly reducing conditions, while oxyfluorene (OF) originates in weakly reducing or oxidizing settings, and fluorene (F) is associated with freshwater to brackish lacustrine environments Zhang and Philp [40]. In the study area, the Es4d3 source rocks exhibit a SF > F > OF triaromatic fluorene series (Table 3 and Fig. 9a), consistent with deposition in reducing to strongly reducing environments. The Es4g displays relatively lower SF content (though still dominant), alongside reduced F and OF proportions, indicating deposition under moderately reducing conditions (Table 3 and Fig. 9a). Notably, the Es4d3 shares high SF content (> 60 %) with the Bazhenov Formation source rocks (R_o = 0.5 – 0.8 %) in the West Siberian Basin, both indicative of strongly reducing environments [41]. However, the Bazhenov Formation contributes hydrocarbons predominantly at high maturity (R_o > 0.8 %), whereas the Es4d3 initiates hydrocarbon generation at low maturity. This divergence is likely controlled by paleoproductivity and burial rates: Rapid subsidence in the Liaohe Depression facilitated early organic matter preservation (Li et al., 2020; [42], whereas prolonged microbial degradation under slow burial in the Bazhenov system necessitated higher thermal maturity to compensate for organic carbon loss [43].

5.2. Sources of hydrocarbon-generating organic matter

The depositional environment of source rocks exerts a primary control on the composition of their hydrocarbon-generating organic matter. $C_{19\text{-}20}TT$ is generally derived from terrestrial higher plants, whereas $C_{21}TT$ originates predominantly from aquatic lower organisms Philp and Gilbert [44]. In the Liaohe Western Depression, a weak positive correlation exists between the Pr/Ph ratio and $C_{19\text{-}20}TT/C_{21}TT$ ratio in the Es4 source rocks (Fig. 9b), suggesting that moderately oxidizing conditions favor enhanced terrestrial higher plant inputs. Consequently, the Es4g (higher Pr/Ph) exhibits greater contributions from terrestrial organic matter, while the Es4d3 (lower Pr/Ph) is dominated by lacustrine aquatic biomass. This interpretation aligns with trends observed in the Pr/n-C_{17} vs. Ph/n-C_{18} cross-plot (Fig. 8a) and is further supported by the elevated abundance of C_{29} regular steranes—a biomarker indicative of terrestrial higher plants—in the Es4g (Fig. 4).

Semi-brackish to hypersaline environments enriched in microbial and algal biomass favor the formation of 9-methylphenanthrene (9-MP), whereas weakly oxic to suboxic settings dominated by terrestrial higher

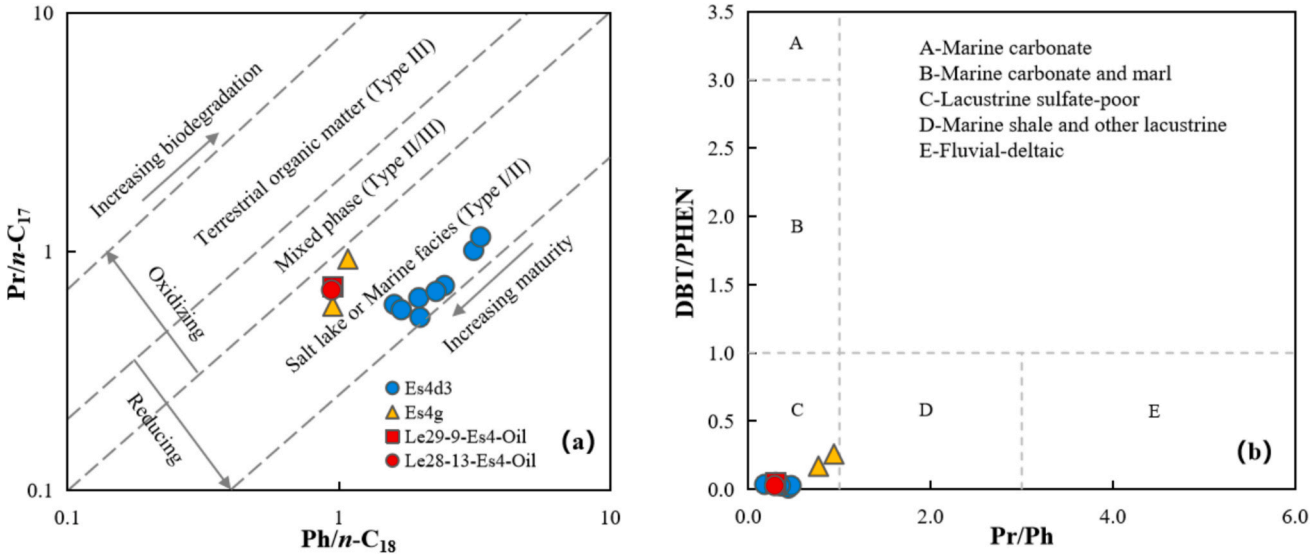

Fig. 8. Cross-plots of (a) Pr/n-C_{17} vs. Ph/n-C_{18} and (b) Pr/Ph vs. DBT/PHEN for the Es4 source rocks and crude oils in the Liaohe Western Depression.

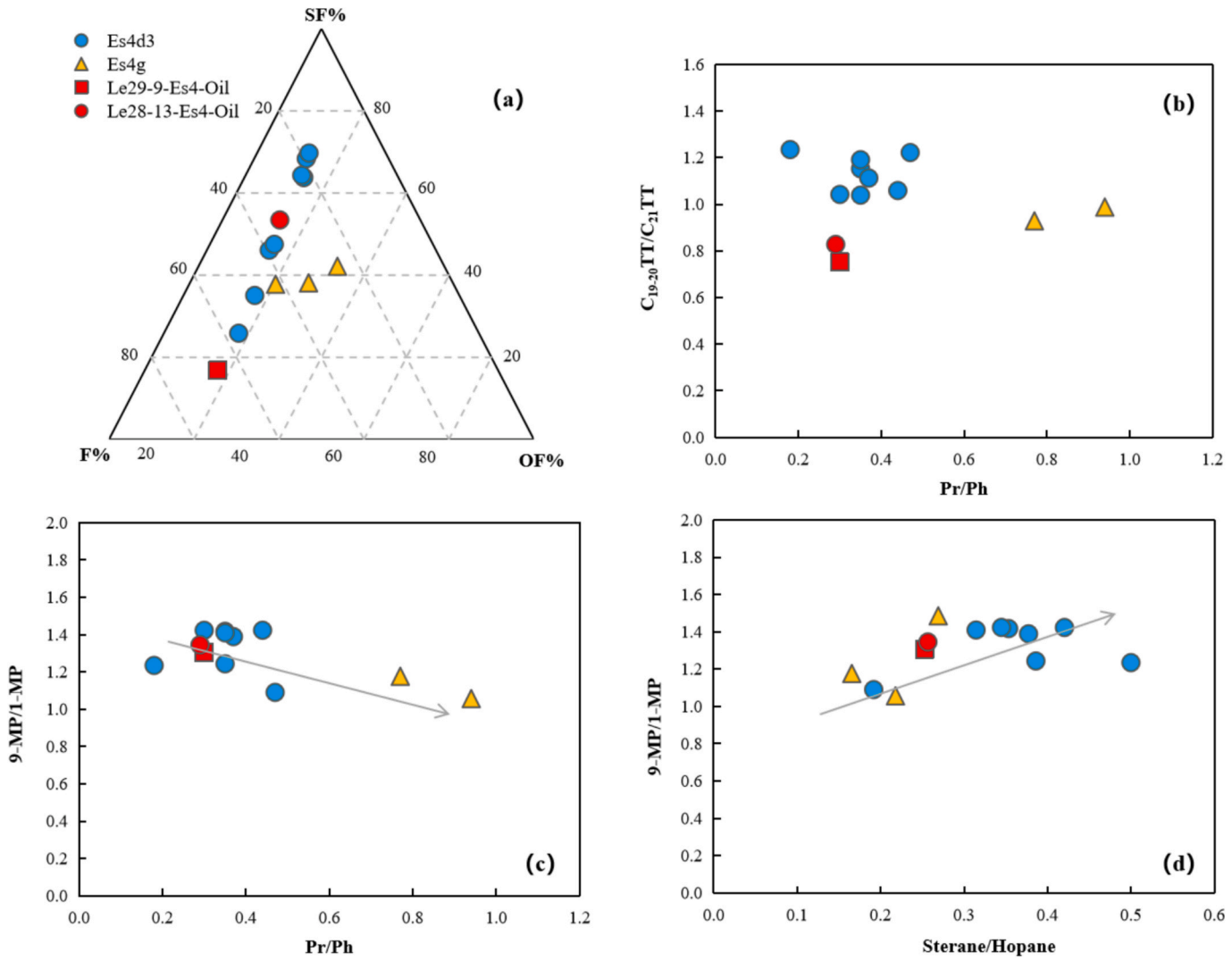

Fig. 9. Geochemical parameter cross-plots for the Es4r source rocks and crude oils in the Liaohe Western Depression: (a) S-SF-OF ternary diagram; (b) $C_{24}Te/C_{26}TT$ vs. Pr/Ph; (c) 9-MP/1-MP vs. Pr/Ph; (d) 9-MP/1-MP vs. sterane/hopane.

plant inputs promote 1-methylphenanthrene (1-MP) generation Radke [45],Zhang and Li [46]. In the Liaohe Western Depression, a negative correlation is observed between the Pr/Ph ratio and the 9-MP/1-MP ratio in the Es4 source rocks (Fig. 9c), indicating algal and microbial-dominated organic matter sources. This interpretation is further corroborated by extremely low dibenzothiophene (DBT) concentrations in the studied samples. Elevated DBT levels typically characterize terrestrial higher plant-derived organic matter, whereas their scarcity here strongly supports aquatic biomass as the primary organic precursor.

Steranes primarily originate from phytosterols derived from eukaryotic organisms (e.g., algae and higher plants), while hopanes are predominantly sourced from bacterial and microbial biomass [47]. Theoretically, a negative correlation is expected between the 9-MP/1-MP ratio (indicative of microbial vs. terrestrial inputs) and the sterane/hopane ratio. However, the Es4 source rocks in the Liaohe Western Depression exhibit a positive correlation between these ratios (Fig. 9d). This anomaly may reflect microbial reworking of terrestrial organic matter during early diagenesis: terrestrial higher plant debris, modified by bacterial activity, became integrated into the hydrocarbon-generating organic matrix alongside microbial biomass [47]. Such microbial-terrestrial synergy likely contributed to the wide $\delta^{13}C$ variability observed in the organic fractions.The Es4d3 source rocks, characterized by lighter $\delta^{13}C$ values (Fig. 6), further support a microbial-algal-dominated organic assemblage, consistent with their deposition in a strongly reducing lacustrine environment that favored preservation of aquatic biomass.

5.3. Oil-source correlation

Molecular geochemical and component-specific carbon isotopic compositions of the Paleogene Es4 crude oils in the western Leijia Depression indicate a predominant origin from the Es4d3 source rocks, as detailed below:

(1) Molecular Geochemical Composition. The two analyzed crude oil samples exhibit molecular signatures closely aligned with the Es4d3 source rocks: Low Pr/Ph ratios and elevated 9-MP/1-MP and sterane/hopane ratios (Fig. 9); Unimodal distribution of *n*-alkanes and inverted "L"-shaped regular sterane profiles (Fig. 4 and Fig. 10); Enriched thiofluorene (SF), phenanthrene (P), and triaromatic steroids (TAS) (Table 3). In contrast, the Es4g is characterized by higher naphthalene content (Fig. 5), further distinguishing its genetic contribution.
(2) Component-Specific Carbon Isotopic Composition. The crude oils from the Es4 exhibit the following $\delta^{13}C$ values: Saturated

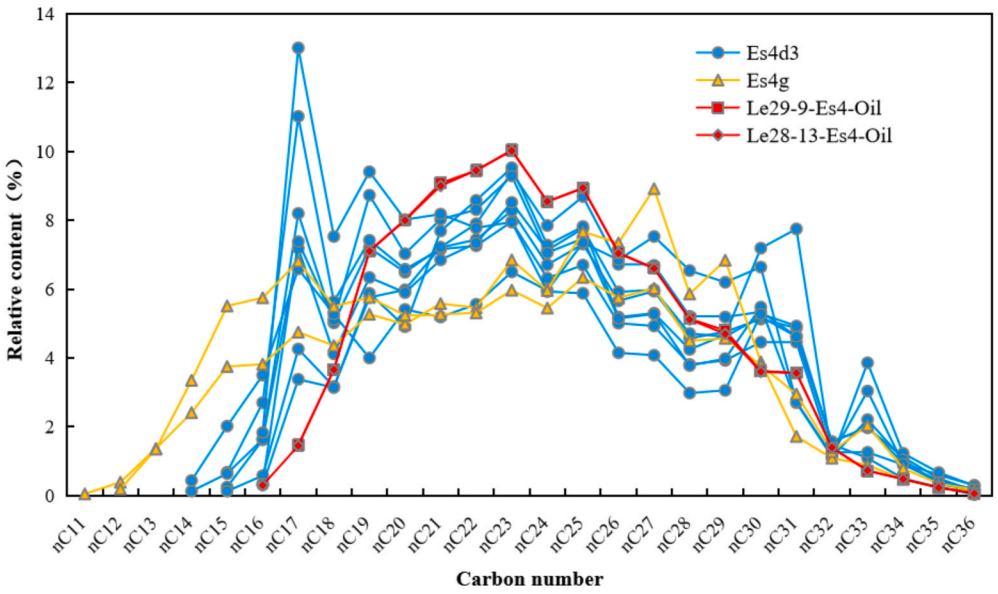

Fig. 10. Distribution characteristics of *n*-alkanes in the Es4 source rocks and crude oils from the Liaohe Western Depression.

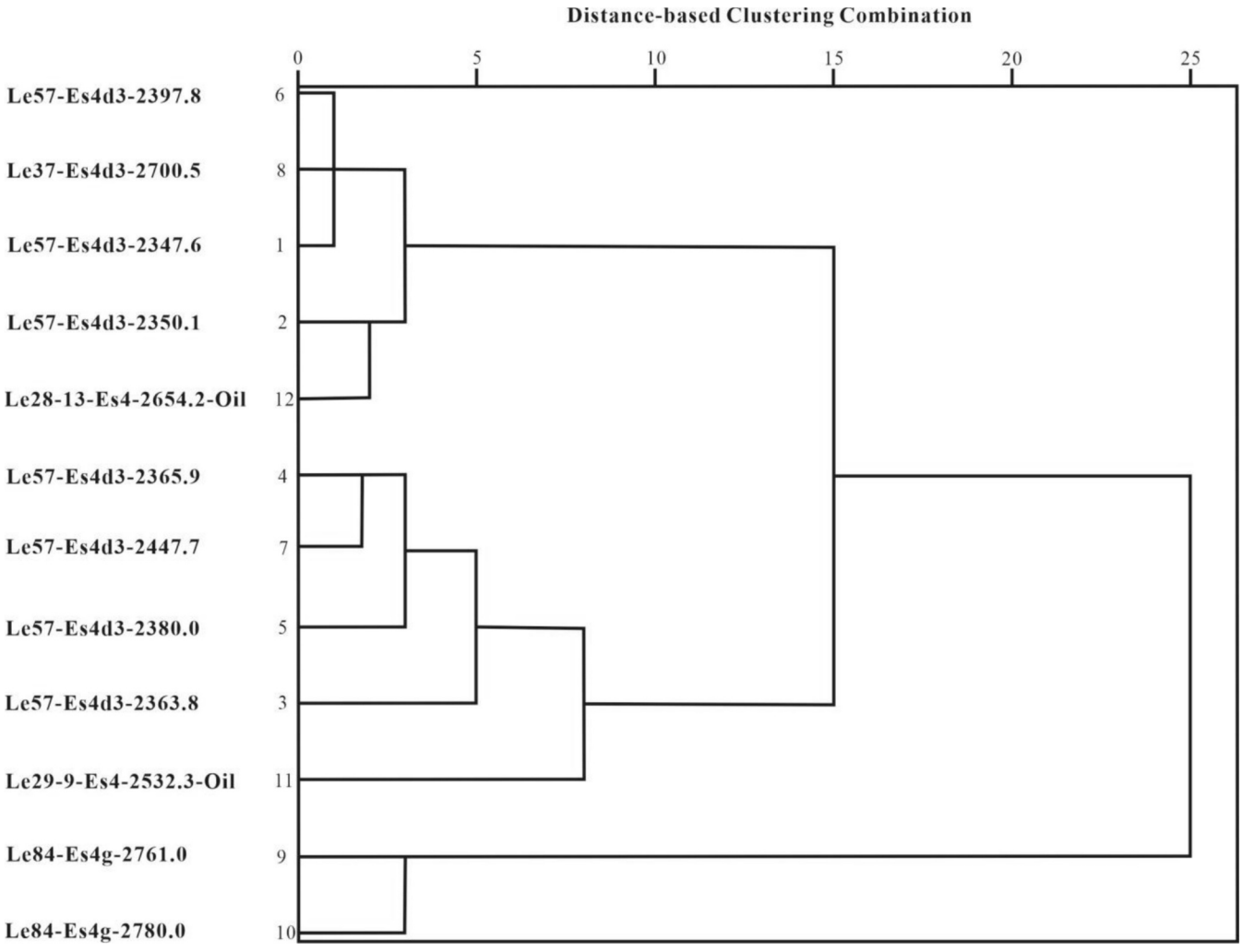

Fig. 11. Hierarchical cluster analysis of source rocks and crude oil samples from the Liaohe Western Depression.

hydrocarbons: −30.3 ‰ to −30.0 ‰; Aromatic hydrocarbons: −28.3 ‰ to −28.2 ‰; Non-hydrocarbons: −28.1 ‰ to −29.0 ‰; Asphaltenes: −28.6 ‰ to −28.3 ‰. The overall lighter $\delta^{13}C$ composition (<-29 ‰) aligns closely with that of the Es4d3 source rocks (Fig. 6), confirming shared organic matter sources dominated by algal and microbial biomass under strongly reducing lacustrine conditions.

(3) Hierarchical Cluster Analysis (HCA). Cluster analysis is a robust method for classifying crude oil types and correlating oil sources, contingent on the selection of effective genetic parameters. This study integrated multiple biomarkers and related indices, selected based on their established diagnostic value for organic matter source, depositional environment, and thermal maturity in lacustrine systems[37]. These included *n*-alkane distributions, steranes, terpanes, phenanthrene and naphthalene series, and triaromatic fluorene series compounds, to perform HCA on source rock (Es4d3 and Es4g) and crude oil samples from the Leijia area. Prior to analysis, all biomarker ratio data were standardized (z-score normalization) to ensure variables with different measurement units and scales contributed equally to the distance calculation[48]. The analysis was performed using IBM SPSS Statistics 27 software with Ward's method and Euclidean distance to assess genetic affinities (Fig. 11). Results demonstrate that the crude oils exhibit stronger genetic ties to the Es4d3 source rocks, likely attributed to their lower activation energies, which facilitated early hydrocarbon generation. In contrast, the higher activation energies of the Es4g may have delayed hydrocarbon generation, resulting in limited contributions to the studied oils. However, the Es4g's high organic matter richness (average TOC = 5.23 %) suggests potential for future deep hydrocarbon exploration.

5.4. Exploration implications

The low activation energy characteristics of the Es4d3 in the western Liaohe Depression (48 – 58 kcal/mol) are comparable to those of the Toolebuc Formation in Australia's Cooper Basin (50 – 54 kcal/mol) but significantly lower than marine shales like the Bakken Formation (58 – 65 kcal/mol) [33]. This disparity reflects synergistic controls by organic matter type and depositional environment: The Bakken Formation (marine Type II kerogen) is dominated by aromatic structures with high thermal stability, requiring elevated maturity for hydrocarbon generation. The Es4d3 (lacustrine Type I–II_1 kerogen) contains algal-derived lipids prone to early cracking, facilitated by lower activation energies. This pattern aligns with observations from other prolific lacustrine systems, such as the Green River Formation (USA; Type I-II kerogen, activation energy typically 50–58 kcal/mol) and the Songliao Basin (China; predominantly Type I kerogen, activation energy often 45–55 kcal/mol), where significant hydrocarbon generation can initiate at lower thermal maturity windows compared to marine shales[49–50], Zhou and Littke [51,52,53]. This discovery provides kinetic justification for exploring low-maturity oils (R_o < 0.7 %) in continental lacustrine basins, complementing the "high-maturity threshold" model of Argentina's Vaca Muerta Formation (55 – 62 kcal/mol) [54]. While the Bakken Formation's tight oil success relies on horizontal drilling, hydraulic fracturing, and brittle reservoir-hosting continuous hydrocarbon generation [55], the Es4d3's low activation energy (favorable for early expulsion) and the Es4g's high TOC (average 5.23 %) suggest distinct strategies: Es4d3: Prioritize "sweet spot" identification in low-activation-energy zones, analogous to Bakken's development model. Es4g: Assess deep thermal evolution (e.g., R_o > 0.8 %) for future resource potential.

It should be noted that our sampling strategy prioritized the central-northern structural units (Chenjia Sag, Gaosheng Uplift, Lengdong Anticline), which, as established by previous studies, host the most prolific tight oil plays within the Es4 Member—specifically the Es4d3 and Es4g oil layers [56],Chen and Yang [57,58]; Wang, 2021). While the western slope facies (with its distinct terrestrial-influenced deposition) and the Es4d1/d2 submembers are not fully represented, our dataset comprehensively captures the two principal hydrocarbon-generating and producing intervals. This focused approach ensures that our geochemical and kinetic models are directly calibrated to and validated against the most economically critical units, providing a robust exploration framework for the core 'sweet spots' in continental rift basins.

6. Conclusions

1 Both the Es4d3 and Es4g represent excellent source rocks with high organic matter richness. The Es4d3 is dominated by Type I–II_1 kerogen at an immature to low-maturity stage (R_o = 0.38–0.54 %), while the Es4g contains Type II_1 kerogen with slightly higher thermal maturity (R_o = 0.46–0.60 %, low-maturity stage).

2 Both sub-members exhibit mixed aquatic-terrestrial organic matter inputs but formed under distinct depositional environments:The Es4d3, deposited in strongly reducing saline lacustrine environments, is dominated by algal and microbial biomass. The Es4g, formed in weakly reducing brackish lacustrine settings, shows greater contributions from terrestrial higher plants

3 Integrated biomarker signatures, compound-specific $\delta^{13}C$ compositions, and hierarchical cluster analysis confirm that the Leijia area crude oils originate predominantly from the Es4d3. This finding expands the spatial distribution of effective source rocks within the Paleogene Es4 and underscores promising hydrocarbon exploration potential in the region

4 Kinetic analysis reveals that the low activation energies of the Es4d3 drive efficient hydrocarbon generation at low-maturity stages, aligning with global lacustrine analogs (e.g., Cooper and Junggar basins). In contrast, the Es4g's higher activation energy necessitates deep thermal evolution modeling to assess its resource potential. The activation energy-source rock coupling model proposed in this study provides a novel parameter for optimizing exploration in continental tight oil systems.

CRediT authorship contribution statement

Zhushi Ge: Writing – original draft. **Xiaoping Liu:** Writing – review & editing. **Xiaoguang Li:** Funding acquisition. **Yongcheng Chen:** Funding acquisition. **Chang Chen:** Funding acquisition. **Zilong Zhang:** Methodology. **Biao Sun:** Investigation. **Yi Zhong:** Software. **Xueyou Tan:** Methodology. **Gaohang Jia:** Resources. **Yu Xia:** Funding acquisition. **Zuowei Li:** Supervision. **Wenhui Xie:** Project administration. **Yu Yuan:** Conceptualization. **Na Gao:** Resources.

Declaration of competing interest

The authors declare that they have no known competing financial interests or personal relationships that could have appeared to influence the work reported in this paper.

Acknowledgements

This work was financially supported by the National Natural Science Foundation of China (Grant No. 42072150) and we thank the sponsors of this project. We sincerely thank the Liaohe Oilfield Exploration and Development Research Institute and the State Key Laboratory of Petroleum Resources and Engineering (China University of Petroleum, Beijing).

Data availability

Data will be made available on request.

References

[1] Jia CZ, Zou CN, Li DH, Zheng M. Assessment criteria, main types, basic features and resource prospects of tight oil in China. Acta Pet Sin 2012;33(3):343–50. https://doi.org/10.7623/syxb201203001.

[2] Brodie MW, Aplin AC, Hart B, Orland IJ, Valley JW, Boyce AJ. Oxygen isotope microanalysis by secondary ion mass spectrometry suggests continuous 300-million-year history of calcite cementation and dolomitization in the Devonian Bakken Formation. J Sediment Res 2018;88(1):91–104. https://doi.org/10.2110/jsr.2018.1.

[3] Hafiz M, Hakhoo N, Bhat GM, Kanungo S, Thusu B, Craig J, et al. Source potential and reservoir characterization of the Cambay Shale, Cambay Basin, India: Implications for tight gas and tight oil resource development. AAPG Bull 2020;104(8):1707–49. https://doi.org/10.1306/03162017174.

[4] Shilov E, Dorhjie DB, Mukhina E, Zvada M, Kasyanenko A, Cheremisin A. Experimental and numerical studies of rich gas Huff-n-Puff injection in tight formation. J Petrol Sci Eng 2022;208:109420. https://doi.org/10.1016/j.petrol.2021.109420.

[5] Yang H, Wu G, Scarselli N, Sun C, Qing H, Han J, et al. Characterization of reservoirs, fluids, and productions from the Ordovician carbonate condensate field in the Tarim Basin, northwestern China. AAPG Bull 2020;104(7):1567–92. https://doi.org/10.1306/02242018060.

[6] Deng J, Liu M, Ji Y, Tang D, Zeng Q, Song L, et al. Controlling factors of tight sandstone gas accumulation and enrichment in the slope zone of foreland basins: the Upper Triassic Xujiahe Formation in Western Sichuan Foreland Basin, China. J Petrol Sci Eng 2022;214:110474. https://doi.org/10.1016/j.petrol.2022.110474.

[7] Alizadeh B, Maroufi K, Fajrak M. Oil-oil correlation, geochemical characteristics, and origin of hydrocarbons from Mansourabad oilfield, SW Iran. J Afr Earth Sc 2018;147:383–92. https://doi.org/10.1016/j.jafrearsci.2018.06.008.

[8] Zheng R, Zhang G, Qu Y, Wang S, Jin X, Chen X, et al. Oil-source correlation under the complex geological conditions: a case study of the Chaiwopu Sag, southern Junggar Basin, NW China. J Petrol Sci Eng 2022;210:110056. https://doi.org/10.1016/j.petrol.2021.110056.

[9] Peters KE, Ramos LS, Zumberge JE, Valin ZC, Scotese CR, Gautier DL. Circum-Arctic petroleum systems identified using decision-tree chemometrics. AAPG Bull 2007;91(6):877–913. https://doi.org/10.1306/12290606097.

[10] Liang T, Jiao ML, Ma XL, Zhang LP. Impacts of mantle-derived fluids on source-related biomarkers in crude oils: a case study from the Dongying Depression, eastern China. Pet Sci 2024;21(6):3706–19. https://doi.org/10.1016/j.petsci.2024.06.002.

[11] Fathy D, Farouk S, Qteishat A, Ahmad F, Sami M, Al-Kahtany K, et al. Geochemical characterization of upper cretaceous organic-rich deposits: Insights from the Azraq basin in Jordan. J Asian Earth Sci 2024;276:106365. https://doi.org/10.1016/j.jseaes.2024.106365.

[12] Liu XY, Chen HH, Xiao XW, Zhang HG, Wang YW, Xu TW, et al. Overpressure evolution recorded in fluid inclusions in the Dongpu depression, Bohai Bay basin, North China. J Earth Sci 2022;33(4):916–32. https://doi.org/10.1007/s12583-020-1375-x.

[13] Hui SS, Pang XQ, Pang H, Li CR, Zhou XL, Hu T, et al. A Data-Driven Approach to the Unified Evaluation of conventional and Unconventional Hydrocarbon Resources: Application to Low-Mature to Mature Source Rocks in the Liaohe Western Depression. Minerals 2023;13(3):390. https://doi.org/10.3390/min13030390.

[14] Fathy D, El-Balkiemy AF, Makled WA, Hosny A. Organic geochemical signals of Paleozoic rocks in the southern Tethys, Siwa basin, Egypt: implications for source rock characterization and petroleum system. Phys Chem Earth, Parts a/b/c 2023;130:103393. https://doi.org/10.1016/j.pce.2023.103393.

[15] Wang W, Zheng K, Huang SQ, Wang QY, Feng GQ, Su Y, et al. Difference of hydrocarbon generation between argillaceous dolomite and mudstone and its influence on oil source: a case study of the es4 in the leijia area, liaohe depression. Geoenergy Sci Eng 2024;237(000):8. https://doi.org/10.1016/j.geoen.2024.212805.

[16] Zhang Z, Bao ZD, Tong HM, Wang Y, Li HW. Tectonic evolution and its control over deposition in fault basins: a case study of the Western Sag of the Cenozoic Liaohe Depression, eastern China. Pet Sci 2013;10:269–81. https://doi.org/10.1007/s12182-013-0276-3.

[17] Wang SY, Li JZ, Wang SJ, Zheng M, Wu XZ. Characteristics of hydrocarbon resource structure in the fourth member of Shahejie Formation in Leijia area, western sag of Liaohe Depression. Nat Gas Geosci 2016;27(9):1728–41. https://doi.org/10.11764/j.issn.1672-1926.2016.09.1728.

[18] Pitt BM. Oxidation of phenylpyruvates to aromatic aldehydes and oxalate. Nature 1962;196(4851):272–3. https://doi.org/10.1038/196272a0.

[19] Braun RL, Burnham AK. Analysis of chemical reaction kinetics using a distribution of activation energies and simpler models. Energy Fuel 1987;1(2):153–61. https://doi.org/10.1021/ef00002a003.

[20] Schenk HJ, Horsfield B. Using natural maturation series to evaluate the utility of parallel reaction kinetics models: an investigation of Toarcian shales and Carboniferous coals. Germany Organic Geochemistry 1998;29(1–3):137–54. https://doi.org/10.1016/S0146-6380(98)00139-9.

[21] Mahlstedt N, Horsfield B, Dieckmann V. Second order reactions as a prelude to gas generation at high maturity. Org Geochem 2008;39(8):1125–9. https://doi.org/10.1016/j.orggeochem.2008.04.011.

[22] Hui SS, Pang XQ, Jiang FJ, Wang CX, Mei SX, Hu T, et al. Quantitative effect of kerogen type on the hydrocarbon generation potential of Paleogene lacustrine source rocks,Liaohe Western Depression,China. Pet Sci 2024;21(1):14–30. https://doi.org/10.1016/j.petsci.2023.09.004.

[23] Zhang YB, Li XB, Wang ZD, Ma DC, Jia XL, Wang D. Genetic analysis of carbon isotope reversal in Ordovician crude oil and group components in Tahe Oilfield, Tarim Basin. Nat Gas Geosci 2022;33(8):1332–43. https://doi.org/10.11764/j.issn.1672-1926.2022.01.017.

[24] Tissot, B. P., Welte, D. H., 1984. Geochemical fossils and their significance in petroleum formation . In Petroleum formation and occurrence. Berlin, Heidelberg: Springer Berlin Heidelberg, 19 93-130. 0.1007/978-3-642-87813-8_8.

[25] Panwar DS, Chaurasia RC, Saxena VK, Singh AK, Akanksha. Geochemical investigation of hydrocarbon generation potential of coal from Raniganj Basin, India. J Pet Explor Prod Technol 2021;11:3627–36. https://doi.org/10.1007/s13202-021-01281-4.

[26] Panwar DS, Chaurasia RC, Akansha, Jena SS. Hydrocarbon generation and gasification study of Valia lignite, Gujrat, India. Energy Sources Part A 2021;47(1):8443–53. https://doi.org/10.1080/15567036.2021.1931567.

[27] Yang, W. L., 1985. Petroleum Geology of the Songliao Terrestrial Basin . Petroleum Industry Press, 219-228. http://www.cgl.org.cn/auto/db/detail.aspx?db=10016&rid=39857.

[28] Panwar DS, Saxena VK, Chaurasia RC, Singh AK. Prospective evaluation of coal bed methane in Raniganj coal field, India. Energy Sources Part A 2017;39(9):946–54. https://doi.org/10.1080/15567036.2017.1279242.

[29] Nath M, Panwar DS, Chaurasia RC, Akanksha. Hydrocarbon generative potential and thermal maturity of newly discovered coal seams from Bapung Coalfield, Meghalaya, India: Rock-Eval pyrolysis and organic petrographic analysis. J Sediment Environ 2023;8(3):297–309. https://doi.org/10.1007/s43217-023-00135-9.

[30] Nath M, Panwar DS, Chaurasia RC, Kaur J, Kohli D. New insight into geochemical characterization of Paleogene coals from Jarain coalfield, Meghalaya, NE India: Hydrocarbon potential and organic petrographic analysis. Geoenergy Sci Eng 2023;226:211790. https://doi.org/10.1016/j.geoen.2023.211790.

[31] Yang SB, Li MJ, Wang YS, Xiao H, Huang SQ, Kang WJ, Wang FZ. Dynamic simulation of gas accumulation processes in faulted lacustrine basins: a case study of Liaohe Depression. Bohai Bay Basin Natural Gas Industry 2023;43(9):73–84. https://doi.org/10.3787/j.issn.1000-0976.2023.09.007.

[32] Gao, Y., Jiang, X., Liu, F., Wang, X. Y., Liu, R. H., 2017. Sedimentary characteristics and formation mechanisms of lacustrine beach-bars in the fourth member of the Shahejie Formation in the Shubei area, western depression of the Liaohe Oilfield, China. J. Earth Sci. 28, 1178–1190 (2017). 10.1007/s12583-016-0928-0.

[33] Jarvie DM, Hill RJ, Ruble TE, Pollastro RM. Unconventional shale-gas systems: the Mississippian Barnett Shale of north-central Texas as one model for thermogenic shale-gas assessment. AAPG Bull 2007;91(4):475–99. https://doi.org/10.1306/12190606068.

[34] Didyk BM, Simoneit BRT, Brassell SC, Eglinton G. Organic geochemical indicators of palaeoenvironmental conditions of sedimentation. Nature 1978;272(5650):216–22. https://doi.org/10.1038/272216a0.

[35] Connan J. Biodegradation of crude oils in reservoirs. Adv Pet Geochem 1984;1:299–335. https://doi.org/10.1016/0079-1946(79)90084-3.

[36] Abdelhady AA, Seuss B, Jain S, Fathy D, Sami M, Ali A, et al. Molecular technology in paleontology and paleobiology: applications and limitations. Quat Int 2024;685:24–38. https://doi.org/10.1016/j.quaint.2024.01.006.

[37] Peters, K. E., Walters, C. C., Moldowan, J. M., 2005. The biomarker guide: Biomarkers and isotopes in petroleum exploration and earth history (2nd ed.). Cambridge University Press. Doi: 10.1017/cbo9781107326040.

[38] Radke M, Welte DH, Willsch H. Geochemical study on a well in the Western Canada Basin: relation of the aromatic distribution pattern to maturity of organic matter. Geochim Cosmochim Acta 1982;46(1):1–10. https://doi.org/10.1016/0016-7037(82)90285-X.

[39] Hughes WB, Holba AG, Dzou LI. The ratios of dibenzothiophene to phenanthrene and pristane to phytane as indicators of depositional environment and lithology of petroleum source rocks. Geochim Cosmochim Acta 1995;59(17):3581–98. https://doi.org/10.1016/0016-7037(95)00225-O.

[40] Zhang M, Philp P. Geochemical characterization of aromatic hydrocarbons in crude oils from the Tarim, Qaidam and Turpan Basins, NW China. Pet Sci 2010;7:448–57. https://doi.org/10.1007/s12182-010-0097-6.

[41] Kontorovich AE, Burshtein LM, Livshits VR, Fomin AN. Petroleum generation in the Bazhenov Formation of the West Siberian Basin. Russ Geol Geophys 2013;54(8):917–28. https://doi.org/10.1016/j.rgg.2013.07.006.

[42] Evgeniya, L., Polina, M., Elena, K., Veniamin, P., Nikita, M., Mikhail, S., 2021. The effect of organic matter maturity on kinetics and product distribution during kerogen thermal decomposition: the Bazhenov Formation case study, J. Petrol. Sci. Eng., 204, 108751, ISSN 0920-4105.

[43] Alexei VM. Methanogenic biodegradation of petroleum in the West Siberian Basin (Russia): significance for formation of giant Cenomanian gas pools. AAPG Bull 2010;94(10):1485–541. https://doi.org/10.1306/01051009122.

[44] Philp RT, Gilbert TD. Biomarker distributions in Australian oils predominantly derived from terrigenous source material. Org Geochem 1986;10(1–3):73–84. https://doi.org/10.1016/0146-6380(86)90010-0.

[45] Radke, Matthias, 1988. Application of aromatic compounds as maturity indicators in source rocks and crude oils. Marine Petrol Geol, 1988, 5(3): 224-236. 10.1016/0264-8172(88)90003-7.

[46] Zhang MM, Li Z. Thermal maturity of the Permian Lucaogou Formation organic-rich shale at the northern foot of Bogda Mountains, Junggar Basin (NW China): Effective assessments from organic geochemistry. Fuel 2018;211:278–90. https://doi.org/10.1016/j.fuel.2017.09.069.

[47] Qian Y, Zhang T, Wang ZD, Tuo JC, Zhang MF, Wu CH, et al. Organic geochemical characteristics and generating potential of source rocks from the Lower-Middle

Jurassic coal-bearing strata in the East Junggar Basin, NW China. Mar Pet Geol 2018;93:113–26. https://doi.org/10.1016/j.marpetgeo.2018.02.036.
[48] Kaufman, L., Rousseeuw, P. J., 2009. Finding groups in data: An introduction to cluster analysis. John Wiley & Sons. 10.1002/9780470316801.
[49] Behar F, Vandenbroucke M, Tang Y, Marquis F, Espitalie J. Thermal cracking of kerogen in open and closed systems: determination of kinetic parameters and stoichiometric coefficients for oil and gas generation. Org Geochem 1997;26(5–6): 321–39. https://doi.org/10.1016/S0146-6380(97)00014-4.
[50] Behar F, Roy S, Jarvie D. Artificial maturation of a Type I kerogen in closed system: Mass balance and kinetic modelling. Org Geochem 2010;41(11):1235–47. https://doi.org/10.1016/j.orggeochem.2010.08.005.
[51] Zhou YS, Littke R. Numerical simulation of the thermal maturation, oil generation and migration in the Songliao Basin. Northeastern China Marine Petrol Geol 1999; 16(8):771–92. https://doi.org/10.1016/S0264-8172(99)00043-4.
[52] Wang M, Lu SF, Xue HT. Kinetic simulation of hydrocarbon generation from lacustrine type I kerogen from the Songliao Basin: Model comparison and geological application. Mar Pet Geol 2011;28(9):1714–26. https://doi.org/10.1016/j.marpetgeo.2011.07.004.
[53] Wang, J., Wang, Q. B., Wang, F. L., Liu, X. J., Pan, W. J., 2017. Experimental Study on Hydrocarbon Generation Simulation by Gold-Tube Pyrolysis of Source Rocks in the Bozhong Area, Bohai Sea. Petrol Geol Exp, 39(3), 8. Doi: 10.11781/sysydz201703423.
[54] Fantín MA, Sánchez ML, González R, Vallejo E. Hydrocarbon generation and retention in the Vaca Muerta Formation, Argentina: Insights from basin modeling. Mar Pet Geol 2020;122:104663. https://doi.org/10.1016/j.marpetgeo.2020.104663.
[55] Sonnenberg SA, Pramudito A. Geology and development of the Bakken Formation, Williston Basin. North Am Mar Petrol Geol 2020;121:104582. https://doi.org/10.1016/j.marpetgeo.2020.104582.
[56] Shan JF, Huang SQ, Li L. Lacustrine carbonate sedimentary environment of Leijia in the western depression of the Liaohe Depression. Special Oil and Gas Reservoirs 2014;21(5):5. https://doi.org/10.3969/j.issn.1006-6535.2014.05.002.
[57] Chen, Y. H., Yang, L., M., Ou, Y. F., Chen, Y. Hu., 2018. The influence of paleotopography before sedimentation on the distribution of favorable reservoirs in tight oil reservoirs: A case study of the Shasi Formation tight oil reservoir in the Leijia area of the Liaohe Depression. Petrol Geol Eng, 32(1), 5. CNKI:SUN:SYHN.0.2018-01-009.
[58] Wang Y, Wang SY, Li JZ, Zhang YJ. Hydrocarbon expulsion efficiency of medium–low maturity source rocks in the Shasi section in the Leijia area, Western Liaoning and exploration prospects for tight oil and shale oil. Pet Explor Dev 2019; 40(4):12.10.11743/ogg20190411.